J. Fluid Mech. (2012), *vol.* 698, *pp.* 406–422. © Cambridge University Press 2012
doi:10.1017/jfm.2012.98

An analytically predictive model for moderately rarefied gas flow

Thomas Veltzke† and Jorg Thöming

Center for Environmental Research and Sustainable Technology (UFT), University of Bremen, Leobener Strasse, 28359 Bremen, Germany

(Received 9 September 2011; revised 22 December 2011; accepted 15 February 2012; first published online 5 April 2012)

In microducts deviation from continuum flow behaviour of a gas increases with rarefaction. When using Navier–Stokes equations to calculate a flow under slightly and moderately rarefied conditions, slip boundary conditions are used which in turn refer to the tangential momentum accommodation coefficient (TMAC). Here we demonstrate that, in the so-called slip and transition regime, the flow in microducts can be reliably described by a consistently non-empirical model without considering the TMAC. We obtain this equation by superposition of convective transport and Fickian diffusion using two-dimensional solutions of Navier–Stokes equations and a description for the Knudsen diffusion coefficient as derived from kinetic theory respectively. For a wide variety of measurement series found in the literature the calculation predicts the data accurately. Surprisingly only size of the duct, temperature, gas properties and inlet and outlet pressure are necessary to calculate the resulting mass flow by means of a single algebraic equation. From this, and taking the discrepancies of the TMAC concerning surface roughness and nature of the gases into account, we could conclude that neither the diffusive proportions nor the total mass flow rates are influenced by surface topology and chemistry at Knudsen numbers below unity. Compared to the tube geometry, the model slightly underestimates the flow rate in rectangular channels when rarefaction increases. Likewise, the dimensionless mass flow rate and the diffusive proportion of the total flow are distinctly higher in a tube. Thus the cross-sectional geometry has a significant influence on the transport mechanisms under rarefied conditions.

Key words: general fluid mechanics, kinetic theory, microfluidics

1. Introduction

The gas flow in microchannels and microtubes has been intensively studied since Maxwell's work 'on stresses in rarified gases' (Maxwell 1879) and the work of Knudsen (1909). The development of micro devices (micro/nano electro mechanical systems, lab-on-a-chip) by new manufacturing techniques has raised the necessity for a deeper understanding of the physical laws governing the fluid flow inside them. In such systems the mean free path of the fluid molecules can be of the same order of magnitude as the height or diameter of the duct. This circumstance causes deviation from continuum flow behaviour and consequently the need for distinct approaches for modelling gas flows at the microscale.

† Email address for correspondence: tveltzke@uni-bremen.de

https://doi.org/10.1017/jfm.2012.98 Published online by Cambridge University Press

Reference	Roughness (nm)	Gas	TMAC
Arkilic, Breuer & Schmidt (2001)	0.65	Ar	0.80
		N_2	0.83
		CO_2	0.88
Maurer *et al.* (2003)	20	He	0.91
		N_2	0.87
Colin *et al.* (2004)	?	He	0.93
		N_2	0.93
Graur *et al.* (2009)	<20	He	0.93
		Ar	0.91
		N_2	0.96
Pitakarnnop *et al.* (2010)	5–8	Ar	1.00
Yamaguchi *et al.* (2011)	?	Ar	0.81
		N_2	0.79

TABLE 1. Experimental tangential momentum accommodation coefficients derived by microduct experiments.

According to Gad-el-Hak (1999) there are basically two possible kinds of model concept: on the one hand the molecular models which consider the molecular nature of a gas and on the other hand the continuum models which ignore it. For the molecular-based calculation of macroscopic flow properties such as mass flow rate and pressure drop, large computational power is needed due to the determination of position, velocity and state of all molecules at all times. Continuum models like Navier–Stokes equations and Burnett equations can be solved comparatively easily with a few simplifying assumptions. Since the gas density and velocity are defined as averages over volume elements that are large in comparison to the molecular nature (Gad-el-Hak 1999), the macroscopic quantities can be predicted reliably. This definition becomes invalid with increasing rarefaction due to the decreasing number of molecules per unit volume. All experiments on rarefied gas flow show that the measured mass flow is higher than predicted by the solution of continuum models (Knudsen 1909; Arkilic 1994; Shih *et al.* 1996; Arkilic, Schmidt & Breuer 1997*a*,*b*; Jang *et al.* 2002). Further this deviation rises with increasing rarefaction (Maurer *et al.* 2003; Colin 2005; Ewart *et al.* 2006, 2007*a*,*b*; Yamaguchi *et al.* 2011).

A compromise to enable use of the continuum models even for rarefied gas flow is the definition of slip boundary conditions unlike the classical wall adherence condition. Myong (2004) derived a slip model based on the Langmuir adsorption isotherm which yields a prediction in good agreement with the experimental data of Shih *et al.* (1996). Commonest in the pertinent literature is the Maxwellian (Maxwell 1879) boundary condition of different high order (Arkilic 1994; Jang *et al.* 2002; Maurer *et al.* 2003; Hsieh *et al.* 2004; Colin, Lalonde & Caen 2004; Colin 2005; Ewart *et al.* 2006; Stevanovic 2007; Graur *et al.* 2009; Pitakarnnop *et al.* 2010; Yamaguchi *et al.* 2011). This slip model considers the molecular nature of the fluid in the distinction of diffusively and specular reflected molecules after a collision with the wall. The fraction of diffusively scattered molecules defines the tangential momentum accommodation coefficient (TMAC). The influence parameters on the TMAC is a controversial issue. In table 1 a variety of references is listed to allow an investigation of the dependence of the TMAC on roughness and the nature of the gas.

https://doi.org/10.1017/jfm.2012.98 Published online by Cambridge University Press

Arkilic *et al.* (2001) and Graur *et al.* (2009) found the TMAC of argon to be significantly lower than of nitrogen. However Yamaguchi *et al.* (2011) found the reverse. Colin *et al.* (2004) measured the TMAC of helium and nitrogen to be identical, unlike Maurer *et al.* (2003) who found the value of helium to be significant higher. Pitakarnnop *et al.* (2010) performed their measurements in rectangular channels with a typical roughness of 5–8 nm which is considerably lower than the surface roughness Graur *et al.* (2009) stated. Nevertheless Pitakarnnop *et al.* (2010) measured the highest TMAC which differs from the common state of the art (Tang *et al.* 2007; Cao, Sun & Guo 2009) as well as molecular dynamic simulations (Cao, Chen & Guo 2006; Sun & Li 2010) and other numerical methods (Sun & Faghri 2003; Ji, Yuan & Chung 2006). Also Agrawal & Prabhu (2008) revealed a crucial dependence of the roughness in their review on TMAC measurements. However Turner *et al.* (2004) investigated the influence of roughness specifically and found no significant effect.

Although the impact of the TMAC on the mass flow might be minor in the moderately rarefied regime, the inconsistencies shown led us to doubt that a TMAC-based approach can describe the observed effects correctly. Furthermore it appears inconsistent to solve differential equations embodying the continuum model with a boundary condition based on the molecular one. Moreover, when using models that are based on the Maxwellian boundary condition, it is impossible to predict the mass flow (or the respective pressure drop) without knowing the TMAC.

Alternative approaches which are based on the superposition of convection and a diffusive component have already been published by Pollard & Present (1948) and Lund & Berman (1966). Since in both references a slip coefficient is used, the same inconsistencies as mentioned above occur.

In several publications it has been shown that directed molecular diffusion can correct deviations from the continuum theory in a predictive manner. Dadzie, Reese & McInnes (2008), Dadzie & Reese (2010) and Dongari *et al.* (2011) for instance modified the classical conservative equations of mass and momentum by a dissipative mass–density flux using Fick's first law of diffusion. Brenner (2011) suggested that slip arises due to gradients in the mass density of the fluid at the wall and presented a mass diffusion boundary condition without using tangential momentum accommodation.

In this paper we present a new analytical model for rarefied gas flow in long rectangular microchannels and microtubes that allows the total mass flow to be divided according to the transport mechanisms. The total flow caused by a pressure gradient is assumed to be a superposition of convection and molecular spatial diffusion. The convection is described by a solution of the Navier–Stokes equations with no-slip boundary condition and for Knudsen diffusion we use Fick's first law including the diffusion coefficient. As both are non-empirical, their superposition is stringently predictive. We can show that the model predicts consistently and reliably the mass flow measured by a variety of authors.

2. Background theory

In this section we focus on the derivation of the model for diffusive transport used in our approach because the explanation of the Navier–Stokes equations, phenomenologically describing the conversion of momentum or deduced from the Boltzmann equation, is well-known in the basic literature (Geankoplis 1972; Sherman 1990; Panton 1996).

https://doi.org/10.1017/jfm.2012.98 Published online by Cambridge University Press

The model of steady diffusive flux is analogous to Ohm's law whereby the flux J corresponds to the current, a local concentration gradient $\partial c/\partial x$ to the voltage and the diffusion coefficient D to the conductivity. This correlation is embodied in Fick's first law (Fick 1855)

$$J = -D\frac{\partial c}{\partial x}, \tag{2.1}$$

where D varies with the kind of diffusion mechanism and thus depends on flow phenomena. A general overview is given by Cussler (2009) and specified for transport in porous solids by Cunningham & Williams (1980) and Kaerger & Ruthven (1992). Directed diffusive transport in a microchannel or microtube can be considered as pore diffusion including bulk, Knudsen and surface diffusion as well as capillary condensation (Cussler 2009), whereby the proportion of each mechanism depends on the ratio of the mean free path of the fluid molecules λ to the pore size. This ratio quantifies the rarefaction of a gas in the form of the mean Knudsen number

$$Kn_m = \frac{\lambda}{s} = \frac{k_B T}{s\sqrt{2}\pi\sigma^2 p_m}, \tag{2.2}$$

where k_B is the Boltzmann constant, T the temperature, σ the diameter of a molecule, s the characteristic length (e.g. pore size, tube diameter) and

$$p_m = \frac{p_i + p_o}{2} \tag{2.3}$$

the mean pressure, where the subscript indices i and o denote the inlet and the outlet of the duct. As λ is the same order of magnitude as s, moving molecules collide statistically more frequently with the duct wall than with other molecules (Cussler 2009). In that case Knudsen diffusion is the dominant diffusive transport mechanism and the corresponding diffusion coefficient D_{Kn} is crucially dependent on molecular collision properties. By means of the simplest distribution of molecule position the diffusion coefficient can be estimated by arguments corresponding to the kinetic theory of rigid spheres.

We consider a volume element containing a large amount of rigidly spherical molecules. Contrary to the random walk of the Brownian motion we assume that the molecules are located solely on the three axes of a Cartesian coordinate system. Hence there are only six possible directions of motion ($\pm x$, $\pm y$ and $\pm z$). The distance between the centres of the volume elements is equal to λ (Cunningham & Williams 1980). As the molecular velocities obey the Maxwellian distribution the arithmetical average of the velocity is

$$\bar{v} = \sqrt{\frac{8RT}{\pi M}}, \tag{2.4}$$

where R is the universal gas constant and M the molar mass. Since the volume element is in contact with adjacent units, change of mass is proportional to the flow of molecules across the boundary A_x. Hence the molar flow rate in one direction of the x-axis of the coordinate system is

$$\dot{n}_x^{\pm} = \pm\frac{1}{6}\lambda A_x \bar{v}\frac{\partial c}{\partial x}, \tag{2.5}$$

with the concentration c in mol per unit volume. The entire change of substance results from the balance of the molar flow rates from the left and the right units across

https://doi.org/10.1017/jfm.2012.98 Published online by Cambridge University Press

the boundary

$$\dot{n}_x = \frac{1}{6}\lambda A_x \bar{v}\frac{\partial c}{\partial x} - \left(-\frac{1}{6}\lambda A_x \bar{v}\frac{\partial c}{\partial x}\right) = \frac{1}{3}\lambda A_x \bar{v}\frac{\partial c}{\partial x}. \tag{2.6}$$

Written in terms of the diffusive flux J as molar flow rate per unit area, (2.6) can be compared with Fick's first law according to (2.1)

$$J = -D\frac{\partial c}{\partial x} = \frac{1}{3}\lambda \bar{v}\frac{\partial c}{\partial x}. \tag{2.7}$$

This comparison yields the diffusion coefficient for Knudsen diffusion D_{Kn} with λ replaced by the characteristic length s and with the average molecule velocity according to (2.4):

$$D = D_{Kn} = \frac{1}{3}s\sqrt{\frac{8RT}{\pi M}}. \tag{2.8}$$

For a microtube it is plain to see that the characteristic length is equivalent to the diameter d. However that does not apply to a rectangular channel with its height h much smaller than its width w. Due to the proportionality of J to s the predicted flux with h as the characteristic length is underestimated. As illustrated in figure 1 the characteristic length corresponds to the conjugate diameter d_e of the coextensive ellipse. Therefore the characteristic length of the rectangular channel is calculated by comparing the area of a rectangle and an ellipse with transverse diameter d_t equal to w

$$wh = \frac{\pi d_e d_t}{4}, \tag{2.9}$$

and with $d_e = s$

$$s = \frac{4h}{\pi}. \tag{2.10}$$

Finally the diffusion coefficient for Knudsen diffusion can be written as

$$D^a_{Kn} = \frac{8h}{3\pi}\sqrt{\frac{2RT}{\pi M}}, \tag{2.11}$$

for the rectangular channel and as

$$D^b_{Kn} = \frac{2d}{3}\sqrt{\frac{2RT}{\pi M}}, \tag{2.12}$$

for the tube. Below, variables and constants concerning the duct geometry are marked with superscript indices a for the rectangular channel and b for the tube.

3. Mathematical modelling

The modelling approach is based on a superposition of two mass transport mechanisms

$$\dot{m} = \dot{m}_C + \dot{m}_D, \tag{3.1}$$

where the subscript indices C and D denote convection and molecular spatial diffusion. Models for both types of transport are derived for each of the two commonest microduct geometries, rectangular channel and tube.

https://doi.org/10.1017/jfm.2012.98 Published online by Cambridge University Press

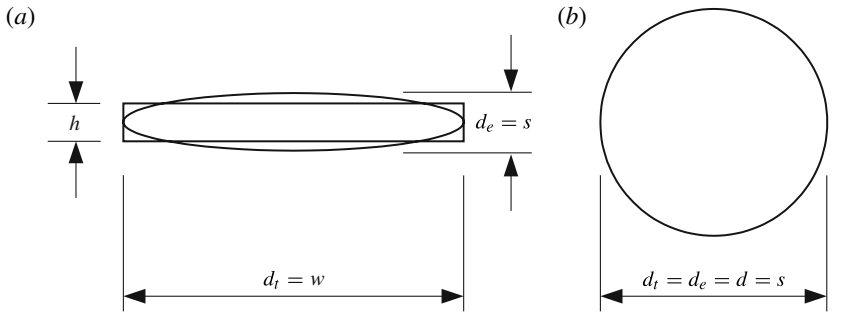


FIGURE 1. Cross-section and geometric properties of rectangular channel (*a*) and tube (*b*).

3.1. *Convection*

A two-dimensional, laminar and steady flow without body forces is considered. According to figure 1 the height h of the rectangular channel is assumed to be much smaller than the width w ($h \ll w$). Further assumptions are expressed in the two boundary conditions for line symmetry of the velocity profile and wall adherence

$$\left.\frac{\partial u}{\partial y}\right|_{y=0} = 0, \quad u|_{y=\pm h/2} = 0; \quad \left.\frac{\partial u}{\partial r}\right|_{r=0} = 0, \quad u|_{r=r^*} = 0, \tag{3.2}$$

where u is the fluid velocity in the direction of the flow and r^* the radius of the tube. The streamwise conservation of momentum for an infinitesimal volume element is given by the Navier–Stokes equation in the x-direction

$$\rho\left(u\frac{\partial u}{\partial x} + u_y\frac{\partial u}{\partial y}\right) = -\frac{\partial p}{\partial x} + \mu\left(\frac{\partial^2 u}{\partial x^2} + \frac{\partial^2 u}{\partial y^2}\right), \tag{3.3}$$

in Cartesian coordinates for the rectangular channel; analogously, for the tube in cylindrical coordinates

$$\rho\left(u_r\frac{\partial u}{\partial r} + \frac{u_\varphi}{r}\frac{\partial u}{\partial \varphi} + u\frac{\partial u}{\partial x}\right) = -\frac{\partial p}{\partial x} + \mu\left(\frac{1}{r}\frac{\partial}{\partial r}\left(r\frac{\partial u}{\partial r}\right) + \frac{1}{r^2}\frac{\partial^2 u}{\partial \varphi^2} + \frac{\partial^2 u}{\partial x^2}\right). \tag{3.4}$$

In (3.3) and (3.4) ρ is the density, μ the dynamic viscosity and p the pressure. While the velocity components in the y-direction, respectively the radial and swirl components are zero for laminar flow, (3.3) and (3.4) reduce to

$$\frac{\partial^2 u}{\partial y^2} = \frac{1}{\mu}\frac{\partial p}{\partial x} \tag{3.5}$$

for the channel and to

$$\frac{1}{r}\frac{\partial}{\partial r}\left(r\frac{\partial u}{\partial r}\right) = \frac{1}{\mu}\frac{\partial p}{\partial x} \tag{3.6}$$

for the tube. Twofold integration yields the velocity u as a function of y and r respectively and two integration constants. For the channel it follows that

$$u^a = \frac{1}{2\mu}\frac{\partial p}{\partial x}y^2 + c_1 y + c_2 \tag{3.7}$$

https://doi.org/10.1017/jfm.2012.98 Published online by Cambridge University Press

and analogously for the tube

$$u^b = \frac{1}{4\mu}\frac{\partial p}{\partial x}r^2 + c_1 \ln(r) + c_2. \tag{3.8}$$

The integration constant c_1 is calculated with the boundary condition for line symmetry (3.2) set to zero. For the second constant it follows that

$$c_2 = \frac{1}{2\mu}\frac{\partial p}{\partial x}\left(\frac{h}{2}\right)^2, \quad c_2 = \frac{1}{4\mu}\frac{\partial p}{\partial x}r^{*2}. \tag{3.9}$$

Utilizing both integration constants the velocity profiles for both geometries can be written as

$$u^a = \frac{1}{2\mu}\frac{\partial p}{\partial x}\left(y^2 - \left(\frac{h}{2}\right)^2\right) \tag{3.10}$$

and

$$u^b = \frac{1}{4\mu}\frac{\partial p}{\partial x}\left(r^2 - r^{*2}\right). \tag{3.11}$$

For the calculation of the flow rate the average velocity $\bar{u}$ is required. By cross-sectional averaging of (3.10) and (3.11) $\bar{u}$ is obtained as

$$\bar{u}^a = \frac{2}{h}\int_{-h/2}^{+h/2}\frac{1}{2\mu}\frac{\partial p}{\partial x}\left(y^2 - \left(\frac{h}{2}\right)^2\right)\mathrm{d}y = \frac{h^2}{12\mu}\frac{\partial p}{\partial x} \tag{3.12}$$

and

$$\bar{u}^b = \frac{1}{\pi r^{*2}}\int_0^{r^*}\frac{2\pi r}{4\mu}\frac{\partial p}{\partial x}\left(r^2 - r^{*2}\right)\mathrm{d}r = \frac{r^{*2}}{8\mu}\frac{\partial p}{\partial x}. \tag{3.13}$$

Note that the pressure drop across the length l of the duct is assumed to be linear ($\Delta p/l$) and thus small so that compression or expansion does not cause significant inequalities of temperature. For a Mach number less than 0.3 the ratio of the mean pressure p_m according to (2.3) to the outlet pressure p_o is used as a correction factor regarding the compressibility of the gaseous fluid (Bird, Stewart & Lightfoot 2007). Multiplying the average velocity $\bar{u}$ with the compressibility correction factor and the cross-section of the duct yields the outlet volumetric flow rate $\dot{V}_o$. The convective mass flow $\dot{m}_C$ can be written in terms of $\dot{V}_o$ based on the equation of state of an ideal gas as

$$\dot{m}_C = \frac{M\dot{V}_o p_o}{RT}. \tag{3.14}$$

Hence (3.12) and (3.13) together with the above-mentioned substitutions applied to (3.14) yields

$$\dot{m}_C^a = \frac{h^3 w M p_m \Delta p}{12\mu RTl} \tag{3.15}$$

for the rectangular channel and

$$\dot{m}_C^b = \frac{\pi d^4 M p_m \Delta p}{128\mu RTl} \tag{3.16}$$

for the tube where $d = 2r^*$ is the tube diameter. This solution of the Navier–Stokes equations is also known as the Hagen–Poiseuille equation for compressible fluids

https://doi.org/10.1017/jfm.2012.98 Published online by Cambridge University Press

(Bird *et al.* 2007).

3.2. *Diffusion*

As shown in the previous section, the steady diffusive flux J is proportional to a local concentration gradient $\partial c/\partial x$, which is the driving force and an arbitrary diffusion coefficient D (2.1). Since the flux is defined as the amount of substance per unit time and cross-section A_x, the diffusive mass flow is

$$\dot{m}_D = JMA_x. \tag{3.17}$$

The concentration c in (2.1) can be expressed by the amount of substance n per unit volume V. With the equation of state of an ideal gas Fick's first law (2.1) is rewritten as

$$J = \left|\frac{D}{RT}\right| \frac{\partial p}{\partial x}. \tag{3.18}$$

Combining (3.17) and (3.18) with the assumption of a linear pressure drop over the length of the duct we write

$$\dot{m}_D = D\frac{MA_x}{RT}\frac{\Delta p}{l}. \tag{3.19}$$

As diffusion coefficient D the coefficient of Knudsen diffusion D_{Kn}, (2.11) and (2.12) derived in the previous section, is used. Applying (2.11) and (2.12) respectively in (3.19) the diffusive mass flow in a rectangular channel can be written as

$$\dot{m}_D^a = \frac{8h^2 w\Delta p}{3\pi l}\sqrt{\frac{2M}{\pi RT}} \tag{3.20}$$

and as an expression which is already stated by Kennard (1938) as

$$\dot{m}_D^b = \frac{d^3\Delta p}{6l}\sqrt{\frac{2\pi M}{RT}} \tag{3.21}$$

for directed diffusive mass flow in a tube. Here it is worth noting that diffusive transport is proportional to cross-section and pressure gradient.

3.3. *Total mass flow*

Superposition of the convective mass flow (3.15) and the diffusive mass flow (3.20) yields

$$\dot{m}^a = \frac{h^3 wMp_m\Delta p}{12\mu RTl} + \frac{8h^2 w\Delta p}{3\pi l}\sqrt{\frac{2M}{\pi RT}} = \frac{h^2 w\Delta p}{3RTl}\left(\frac{hMp_m}{4\mu} + \frac{8}{\pi}\sqrt{\frac{2MRT}{\pi}}\right) \tag{3.22}$$

for the rectangular channel and with (3.16) and (3.21)

$$\dot{m}^b = \frac{\pi d^4 Mp_m\Delta p}{128\mu RTl} + \frac{d^3\Delta p}{6l}\sqrt{\frac{2\pi M}{RT}} = \frac{d^3\Delta p}{2RTl}\left(\frac{\pi dMp_m}{64\mu} + \frac{1}{3}\sqrt{2\pi MRT}\right) \tag{3.23}$$

for the tube. The mass flow is put into a non-dimensional form using the Reynolds number

$$Re^a = \frac{\rho_o \dot{V}_o h}{\mu A} = \frac{\dot{m}^a}{\mu w}, \tag{3.24}$$

https://doi.org/10.1017/jfm.2012.98 Published online by Cambridge University Press

$$Re^a = \frac{h^2 p_o}{3\mu RTl}\left(\frac{hMp_o}{8\mu}(P^2-1)+\frac{8}{\pi}\sqrt{\frac{2MRT}{\pi}}(P-1)\right) \tag{3.25}$$

as a function of the pressure ratio $P = p_i/p_o$; analogously for the tube

$$Re^b = \frac{\rho_o \dot{V}_o d}{\mu A} = \frac{4\dot{m}^b}{\pi\mu d}; \tag{3.26}$$

$$Re^b = \frac{d^2 p_o}{\mu RTl}\left(\frac{dMp_o}{64\mu}(P^2-1)+\frac{2}{3}\sqrt{\frac{2MRT}{\pi}}(P-1)\right). \tag{3.27}$$

Furthermore, another dimensionless mass flow rate S is introduced as the ratio of the total mass flow (3.22) to the convective proportion according to (3.15)

$$S^a = \frac{\dot{m}^a}{\dot{m}^a_C} = 1 + \frac{32\mu}{\pi h M p_m}\sqrt{\frac{2MRT}{\pi}}. \tag{3.28}$$

The mean pressure p_m according to (2.3) can be expressed by means of the mean Knudsen number Kn_m as a measure of the rarefaction. Equation (2.2) is reconverted to p_m and applied in (3.28)

$$S^a = 1 + 64\frac{\mu\sigma^2 Kn_m}{k_B}\sqrt{\frac{R}{\pi MT}}, \tag{3.29}$$

and analogously for the tube

$$S^b = \frac{\dot{m}^b}{\dot{m}^b_C} = 1 + \frac{64\mu}{3\pi d M p_m}\sqrt{2\pi MRT} = 1 + \frac{128\pi}{3}\frac{\mu\sigma^2 Kn_m}{k_B}\sqrt{\frac{R}{\pi MT}}. \tag{3.30}$$

The predicted dimensionless mass flow rate is independent of any geometrical property such as length, diameter, width and height and is also independent of the driving force (P or Δp). Only the gas ($\mu(T)$, σ, M) affects S. A comparison of (3.29) and (3.30) shows that the only difference consists of a constant factor (64 and $128\pi/3$) which is approximately two times higher for the tube.

As mentioned earlier, we consider the diffusive proportion in the total mass flow rate as increasing with rarefaction. Thus the diffusive proportion X is introduced as the ratio of the diffuse mass flow rate (3.20) and (3.21) to the total mass flow rate (3.22) and (3.23). For the rectangular channel we obtain

$$X^a = \frac{\dot{m}^a_D}{\dot{m}^a} = \left(\frac{\pi h p_m}{32\mu}\sqrt{\frac{\pi M}{2RT}}+1\right)^{-1} = \left(\frac{1}{64}\frac{k_B}{\mu\sigma^2 Kn_m}\sqrt{\frac{\pi MT}{R}}+1\right)^{-1} \tag{3.31}$$

and analogously

$$X^b = \frac{\dot{m}^b_D}{\dot{m}^b} = \left(\frac{3dp_m}{64\mu}\sqrt{\frac{\pi M}{2RT}}+1\right)^{-1} = \left(\frac{3}{128\pi}\frac{k_B}{\mu\sigma^2 Kn_m}\sqrt{\frac{\pi MT}{R}}+1\right)^{-1} \tag{3.32}$$

for the tube. According to (3.31) and (3.32), $X^{a,b}$ rises as well as increasing rarefaction with rising viscosity of the gas. This is reasonable due to the inversely proportional dependence of the convective flow (3.15) and (3.16) on the viscosity. Since the viscosity of a gas increases with the power of 0.5 with temperature (Atkins & De Paula 2006), the diminishing influence of the temperature is compensated or overcompensated when using the formula of Sutherland (1895).

https://doi.org/10.1017/jfm.2012.98 Published online by Cambridge University Press

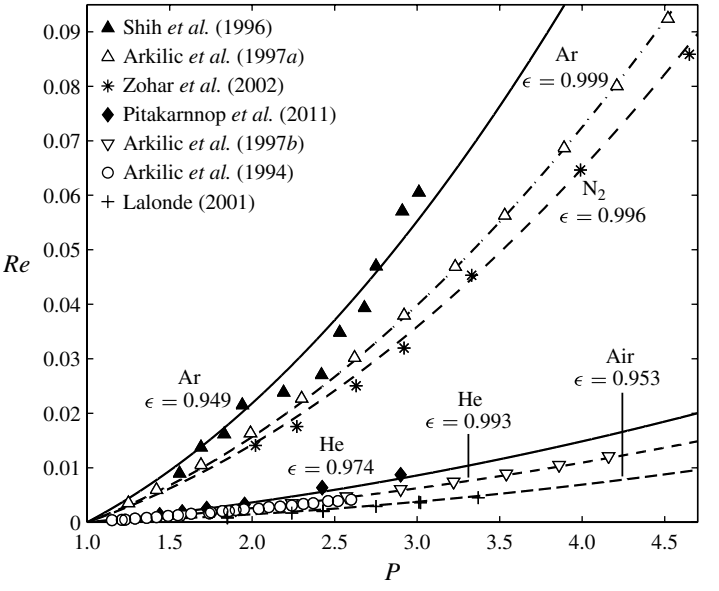


FIGURE 2. Mass flow rate given as Reynolds number versus pressure ratio P for various channel geometries, gases, temperatures (table 2) and outlet pressures. Comparison of experimental data (symbols) and predictions (lines) yields the coefficient of determination ϵ close to unity. The experimental outlet pressure was kept constant at: ▲,⁕,▽,○, $p_o = 100$ kPa; △, 101.3 kPa; ♦, 50 kPa and +, 102.7 kPa.

3.4. *Quality of the model*

To quantify the quality of the presented model, the coefficient of determination ϵ is used. According to Steel & Torrie (1980) ϵ is defined as

$$\epsilon = 1 - \frac{\sum_{j=1}^{n} (\gamma_j - \hat{\gamma}_j)^2}{\sum_{j=1}^{n} (\gamma_j - \bar{\gamma})^2}, \tag{3.33}$$

where γ_j is the value of the data point (Re, S and X), $\bar{\gamma}$ is the average of these and $\hat{\gamma}_j$ is the predicted value calculated with (3.25) and (3.27) for $Re^{a,b}$, (3.29) and (3.30) for $S^{a,b}$ and (3.31) and (3.32) for $X^{a,b}$.

4. Prediction of experimental data

The derived model is applied to the prediction of experimental data of gaseous flows in microchannels and microtubes. The experiments we refer to were performed under isothermal conditions around room temperature with helium, argon, nitrogen and air as working gases (table 2). The Reynolds number and the Mach number were consistently low so that our stated assumptions (§ 3) are complied with.

Figure 2 shows the Reynolds number as a non-dimensional measure of the mass flow rate as a function of the pressure ratio P. The experimental mass flows are extracted from the given literature and non-dimensionalised according to (3.24) for the microchannel experiments and according to (3.26) for the microtube data of Lalonde

https://doi.org/10.1017/jfm.2012.98 Published online by Cambridge University Press

References	Geometry and size Rect., h; w (μm)	l (mm)	Gases	T (K)
Arkilic (1994)	1.33; 52.25	7.5	He	314
Arkilic *et al.* (1997*a*)	1.33; 52.25	7.5	He	314
Ewart *et al.* (2007*a*)	9.38; 492	9.39	He	∼296
Pitakarnnop *et al.* (2010)	1.88; 21.1	5	He, Ar	298.5
Arkilic (1997)	1.33; 52.3	7.49	Ar	293
Arkilic *et al.* (1997*b*)	1.33; 52.25	7.5	Ar	298∗
Shih *et al.* (1996)	1.2; 40	4	Ar	293
Graur *et al.* (2009)	9.38; 492	9.39	Ar, N_2	∼293
Zohar *et al.* (2002)	0.53, 0.97; 40;	4	Ar, N_2	293
	Circ., d (μm)			
Ewart *et al.* (2007*b*)	25.27	53	He, Ar, N_2	298∗
Perrier *et al.* (2011)	49.6	18.2	He, Ar, N_2	296.5
Ewart *et al.* (2006)	25.2	53	N_2	296.5
Yamaguchi *et al.* (2011)	535.6	46.9	N_2	293
Lalonde (2001)	3.9, 20.3, 52.8	20.4, 20.4, 100	Air	294, 298

TABLE 2. Values of parameters in gas flow experiments. The temperatures marked with ∗ were not stated in the primary literature and are assumed as room temperature (298 K).

Gas	M (g mol^{-1})	σ (pm)	μ (10^{-5} Pa s)		
			293 K	298 K	314 K
He	4.003	255.1	1.997	2.019	2.088
Ar	39.95	354.2	2.255	2.286	(2.383)
N_2	28.01	379.8	1.746	1.769	(1.841)
Air	28.96	373.1	1.812	1.836	(1.912)

TABLE 3. Properties of gases used in the cited literature. The molecular diameter of air is calculated as the weighted average of the diameters of N_2 and O_2. The values for the molecular diameter are taken from Cussler (2009). The values in brackets are unused here but stated for completeness.

(2001). The geometries of the ducts required for these calculations are specified in table 2 and the dynamic viscosities are given in table 3. For the microduct experiments shown in figure 2 the outlet pressure p_o was always kept constant. The quality of the simulation is quantified by the value of ϵ according to (3.33) which clearly shows that all experimental data are invariably well predicted.

Comparing for example argon flows in rectangular channels, the channel of Shih *et al.* (1996), although smaller in cross-section, yielded a higher flux compared to the channel of Arkilic *et al.* (1997*b*), which is due to the smaller length. Also comparable are the data of Arkilic *et al.* for helium and argon generated in the same channel. Due to the distinctly higher molar mass and the lower temperature (see (3.25)) the argon flow is much higher despite identical outlet pressure.

While the model for convective gas flow at laminar and subsonic conditions (3.15) and (3.16) is proportional to the product of mean pressure and pressure difference, the diffusive mass flow according to Fick's first law is merely proportional to the pressure

https://doi.org/10.1017/jfm.2012.98 Published online by Cambridge University Press

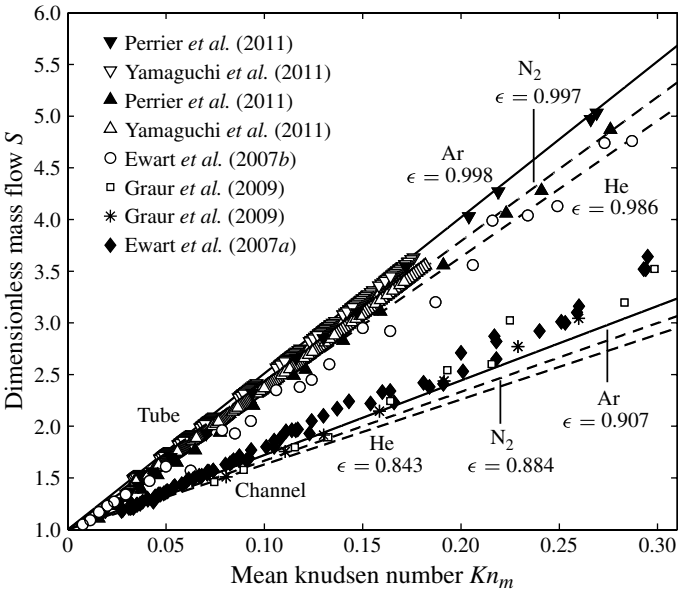


FIGURE 3. Dimensionless mass flow rate as a function of the rarefaction and appendant prediction (lines). Predictions are calculated with $T = 298$ K and values given in table 3.

difference (3.20) and (3.21). Therefore the diffusive proportion of the total flow is high when the mean pressure is low, which is synonymous with a high rarefaction. For high absolute pressures or large pressure gradients the convective transport is dominant. For an evaluation of the derived model over a wide range of rarefaction, the dimensionless mass flow rate S as the measured mass flow rate divided by the Hagen–Poiseuille equation for compressible fluids (3.15) and (3.16) is plotted versus the mean Knudsen number. Figure 3 shows the data points given in literature and the corresponding predictions for tube and channel at room temperature. While S can be exactly predicted for the tube, the data points of the rectangular channels diverge from the simulation with increasing rarefaction. Due to the consistency of that divergence this seems to be a weakness of the model for the rectangular channel.

Since the diffusive proportion X and S are linked for the channel according to

$$X^a = \frac{\dot{m}_D^a}{S\dot{m}_C^a} = \frac{1}{S}\frac{64\mu\sigma^2 Kn_m}{k_B}\sqrt{\frac{R}{\pi MT}} \tag{4.1}$$

and respectively for the tube as

$$X^b = \frac{\dot{m}_D^b}{S\dot{m}_C^b} = \frac{1}{S}\frac{128\pi\mu\sigma^2 Kn_m}{3k_B}\sqrt{\frac{R}{\pi MT}}, \tag{4.2}$$

the divergence is also visible in figure 4 where X is plotted versus the mean Knudsen number. The data points in figure 4 (rectangular channel) and figure 5 (tube) are calculated as the diffusive mass flow rate (3.20) or (3.21) divided by the measured mass flow rate. In contrast to the quite low accordance of data and prediction for the rectangular channel in figure 4, the model fits the data of the tube experiments exactly. The comparison of figures 4 and 5 yields two interesting findings: the experimental diffusive proportion in the rectangular channel is significantly smaller than in the tube

https://doi.org/10.1017/jfm.2012.98 Published online by Cambridge University Press

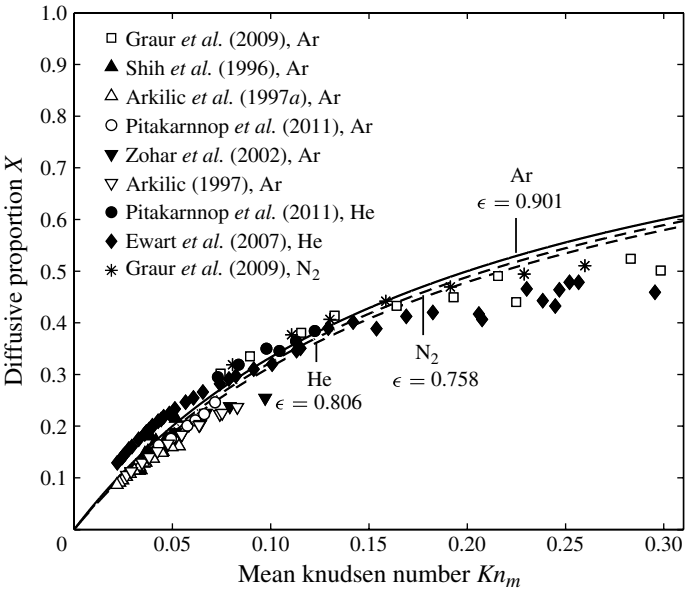


FIGURE 4. Diffusive proportion as a function of the rarefaction and corresponding prediction (lines) for rectangular channels. Predictions are calculated with $T = 298$ K and values given in table 3.

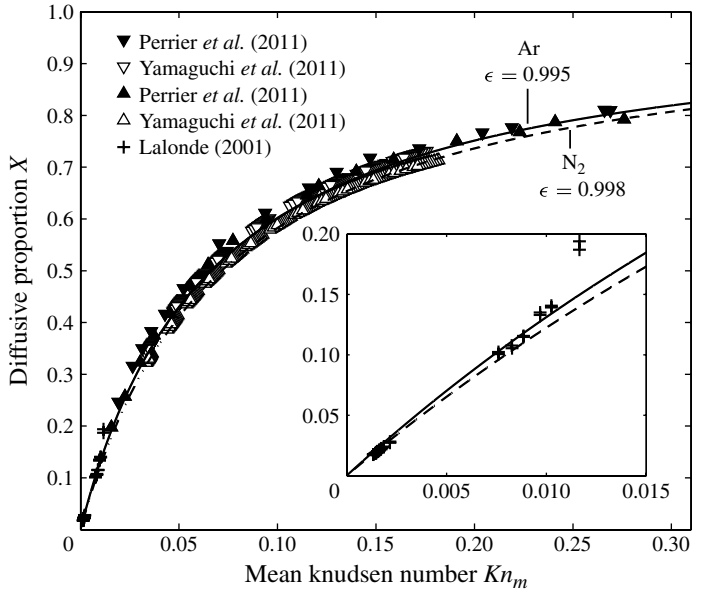


FIGURE 5. Diffusive proportion as a function of the rarefaction and corresponding prediction (lines) for tubes. Predictions are calculated with $T = 298$ K and values given in table 3.

and is also diverging from the prediction. We suppose that diffusion is dependent on the duct geometry due to the ratio of volume and area of the wall. As that ratio is

https://doi.org/10.1017/jfm.2012.98 Published online by Cambridge University Press

a minimum for the tube, it reaches the maximal diffusive proportion. Probably, there is an influence of the wall at higher Knudsen numbers which affects other diffusion mechanisms (Malek & Coppens 2003; Cussler 2009) which are negligible in the non-rarefied and slightly rarefied regime.

Nevertheless figure 4 shows as clearly as figure 3 and figure 5 the dependence of the diffusive proportion of the total flux on the rarefaction in the regime of slightly and moderately rarefied gas flows.

5. Concluding remarks

A consistently predictive model is presented for the analytical calculation of microduct gas flows at low Mach number. The mass flow is modelled as a simple superposition of convective transport and Fickian diffusion. The model is applied to the simulation of experimental results given in the literature. For all measurement series on microtubes the simulation fits the data points accurately, which yields two conclusions:

(i) First, a prediction of the mass flow is possible without the assumption of wall slip in the so-called slip and transition regime (Gad-el-Hak 1999). Knowing the size of the duct, the temperature, the gas properties and the inlet and outlet pressure, the resulting mass flow can be calculated without any adaption parameter, such as the TMAC.

(ii) Second, the classification of non-rarefied into moderately rarefied gas flows in continuum, slip and transition regimes becomes obsolete when the flow is considered as a superposition of different flow mechanisms over the whole range of Knudsen numbers.

For rectangular channels data and model diverge with increasing rarefaction ($Kn > 0.15$). Nevertheless, predictions in the slip regime and the beginning of the transition regime are accurate throughout.

By means of the derived model it could be shown that the diffusive proportion and likewise the dimensionless mass flow rate are not influenced by any variable regarding the surface topology. As a consequence of the broadly varying surface roughness (table 1) of the ducts the cited authors used, we confirm the results of Turner *et al.* (2004) thus far, that surface roughness has no influence on mass transfer in slightly and moderately rarefied gas flows. Further the inconsistencies concerning the dependence of the TMAC on the roughness that we summarized in § 1 lead to reasonable doubts about the slip boundary condition and the state-of-the-art approach in modelling flow processes. Nevertheless there might be an influence of roughness at higher Knudsen numbers due to additionally superimposed self-diffusion which is dependent on molecular residence times at the wall (Malek & Coppens 2003).

Regarding the hypothesis that the TMAC is dependent on the nature of the gas and on the material of the duct (Agrawal & Prabhu 2008), experiments with gases including strong interactions with the surface should be performed. For glass or silica ducts measurements with use of gases with a quadrupole moment (e.g. CO_2) or a permanent dipole (e.g. SO_2, CHF_3) should clarify if rarefied phenomena depend on molecular surface scattering caused by gas–surface interactions.

Finally it was clearly shown that the geometry (rectangular and circular) has a significant influence on the diffusive proportion of the total flux and on the dimensionless mass flow rate. Unfortunately only these two geometries have been commonly used for microflow experiments. We suppose that Fickian diffusion

https://doi.org/10.1017/jfm.2012.98 Published online by Cambridge University Press

becomes more dominant if the shape of the cross-section approaches a circular shape. We postulate that the diffusive proportion of mass flow data obtained from experiments on pentagonal or higher-sided polygonal ducts will lie in between those of tubes and rectangular channels.

Acknowledgements

This work was supported by German Research Foundation (DFG) within the Research Training Group 1375 'Non-metallic Porous Structures for Physical–Chemical Functions'.

REFERENCES

AGRAWAL, A. & PRABHU, S. V. 2008 Survey on measurement of tangential momentum accommodation coefficient. *J. Vac. Sci. Technol.* A **26**, 634–645.

ARKILIC, E. B. 1994 Gaseous flow in micron-sized channels. Master's thesis, Massachusetts Institute of Technology, Cambridge, MA.

ARKILIC, E. B. 1997 Measurement of the mass flow and tangential momentum accommodation coefficient in silicon micromachined channels. PhD thesis, Massachusetts Institute of Technology, Cambridge, MA.

ARKILIC, E. B., BREUER, K. S. & SCHMIDT, M. A. 2001 Mass flow and tangential momentum accommodation in silicon micromachined channels. *J. Fluid Mech.* **437**, 29–43.

ARKILIC, E. B., SCHMIDT, M. A. & BREUER, K. S. 1997*a* Gaseous slip flow in long microchannels. *J. Microelectromech. Syst.* **6**, 167–178.

ARKILIC, E. B., SCHMIDT, M. A. & BREUER, K. S. 1997*b* TMAC measurement in silicon micromachined channels. In *Proceedings of 20th Symposium on Rarefied Gas Dynamics, Bejiing*. Peking University Press.

ATKINS, P. & DE PAULA, J. 2006 *Physical Chemistry*, 8th edn. Oxford University Press.

BIRD, R. B., STEWART, W. E. & LIGHTFOOT, E. N. 2007 *Transport Phenomena*, 2nd edn. John Wiley and Sons.

BRENNER, H. 2011 Beyond the no-slip boundary condition. *Phys. Rev.* E **84**, 046309.

CAO, B.-Y., CHEN, M. & GUO, Z.-Y. 2006 Effect of surface roughness on gas flow in microchannels by molecular dynamics simulation. *Intl J. Engng Sci.* **44**, 927–937.

CAO, B.-Y., SUN, J. & GUO, Z.-Y. 2009 Molecular momentum transport at fluid-solid interfaces in MEMS/NEMS: A review. *Intl J. Mol. Sci.* **10**, 4638–4706.

COLIN, S. 2005 Rarefaction and compressibility effects on steady and transient gas flows in microchannels. *Microfluid Nanofluid* **1**, 268–279.

COLIN, S., LALONDE, P. & CAEN, R. 2004 Validation of a second-order slip flow model in rectangular microchannels. *Heat Transfer Engng* **25**, 23–30.

CUNNINGHAM, R. E. & WILLIAMS, R. J. J. 1980 *Diffusion in Gases an Porous Media*. Plenum.

CUSSLER, E. L. 2009 *Diffusion-Mass Transfer in Fluid Systems*, 3rd edn. Cambridge University Press.

DADZIE, S. K. & REESE, J. M. 2010 A volume-based hydrodynamic approach to sound wave propagation in a monatomic gas. *Phys. Fluids* **22**, 016103.

DADZIE, S. K., REESE, J. M. & MCINNES, C. R. 2008 A continuum model of gas flows with localized density variations. *Physica* A **387**, 6079–6094.

DONGARI, N., DADZIE, S. K., ZHANG, Y. & REESE, J. M. 2011 Isothermal micro-channel gas flow using a hydrodynamic model with dissipative mass flux. In *Rarefied Gas Dynamics: 27th International Symposium.* 1333, pp. 718–724. AIP.

EWART, T. P., PERRIER, P., GRAUR, I. A. & MEOLANS, J. G. 2006 Mass flow rate measurements in gas micro flows. *Exp. Fluids* **41**, 487–498.

EWART, T. P., PERRIER, P., GRAUR, I. A. & MEOLANS, J. G. 2007*a* Mass flow rate measurements in a microchannel, from hydrodynamic to near free molecular regimes. *J. Fluid Mech.* **584**, 337–356.

https://doi.org/10.1017/jfm.2012.98 Published online by Cambridge University Press

EWART, T. P., PERRIER, P., GRAUR, I. A. & MEOLANS, J. G. 2007*b* Tangential momemtum accommodation in microtube. *Microfluid Nanofluid* **3**, 689–695.

FICK, A. 1855 Ueber diffusion. *Ann. Phys.* **170**, 59–86.

GAD-EL-HAK, M. 1999 The fluid mechanics of microdevices – The Freeman scholar lecture. *Trans. ASME: J. Fluids Engng* **121**, 5–33.

GEANKOPLIS, J. G. 1972 *Mass Transport Phenomena*. Holt, Rinehart and Winston.

GRAUR, I. A., PERRIER, P., GHOZLANI, W. & MEOLANS, J. G. 2009 Measurements of tangential momentum accommodation coefficient for various gases in plane microchannel. *Phys. Fluids* **21**, 102004.

HSIEH, S.-S., TSAI, H.-H., LIN, C.-Y, HUANG, C.-F. & CHIEN, C.-M. 2004 Gas flow in a long microchannel. *Intl J. Heat Mass Transfer* **47**, 3877–3887.

JANG, J., ZHAO, Y., WERELEY, S. T. & GUI, L. 2002 Mass flow measurement of gases in deep-RIE microchannels. In *Proceedings of IMECE2002 ASME International Mechanical Engineering Congress & Exposition, New Orleans, Louisiana*, pp. 17–22. ASME.

JI, Y., YUAN, K. & CHUNG, J. N. 2006 Numerical simulation of wall roughness on gaseous flow and heat transfer in a microchannel. *Intl J. Heat Mass Transfer* **49**, 1329–1339.

KAERGER, J. & RUTHVEN, D. M. 1992 *Diffusion in Zeolites and Other Microporous Solids*. Wiley-Interscience.

KENNARD, E. H. 1938 *The Kinetic Theory of Gases*. McGraw-Hill.

KNUDSEN, M. 1909 Die Gesetze der Molekularstroemung und der inneren Reibungsstroemung der Gase durch Roehren. *Ann. Phys.* **333**, 75–130.

LALONDE, P. 2001 Etude experimentale d' ecoulements gazeux dans les microsystemes et fluides. PhD thesis, Institut National des Sciences Appliquees, Tolouse, France.

LUND, L. M. & BERMAN, A. S. 1966 Flow and self-diffusion of gases in capillaries. Part I. *J. Appl. Phys.* **37**, 2489–2495.

MALEK, K. & COPPENS, M.-O. 2003 Knudsen self- and Fickian diffusion in rough nanoporous media. *J. Chem. Phys.* **119**, 2801–2811.

MAURER, J., TABELING, P., JOSEPH, P. & WILLAIME, H. 2003 Second-order slip laws in microchannels for helium and nitrogen. *Phys. Fluids* **15**, 2613–2621.

MAXWELL, J. C. 1879 On stresses in rarified gases arising from inequalities of temperature. *Phil. Trans. R. Soc. Lond.* **170**, 231–256.

MYONG, R. S. 2004 Gaseous slip models based on the Langmuir adsorption isotherm. *Phys. Fluids* **16**, 104–117.

PANTON, R. L. 1996 *Incompressible Flow*, 2nd edn. Wiley-Interscience.

PERRIER, P., GRAUR, I. A., MEOLANS, T. & EWART, J. G. 2011 Mass flow rate measurements in microtubes: From hydrodynamic to near free molecular regime. *Phys. Fluids* **23**, 042004.

PITAKARNNOP, J., VAROUTIS, S., VALOUGEORGIS, D., GEOFFROY, S., BALDAS, L. & COLIN, S. 2010 A novel experimental setup for gas microflows. *Microfluid Nanofluid* **8**, 57–72.

POLLARD, W. G. & PRESENT, R. D. 1948 On gaseous self-diffusion in long capillary tubes. *Phys. Rev.* **73**, 762–774.

SHERMAN, F. S. 1990 *Viscous Flow*. McGraw-Hill.

SHIH, J., HO, C., LIU, J. & TAI, Y. 1996 Monoatomic and polyatomic gas flow through uniform microchannels. In *Application of Microfabrication to Fluid Mechanics, ASME Winter Annual meeting, Atlanta, GA*, pp. 197–203. ASME.

STEEL, R. G. & TORRIE, J. H. 1980 *Principles and Procedures of Statistics: A Biometrical Approach*, 2nd edn. McGraw-Hill.

STEVANOVIC, N. D. 2007 A new analytical solution of microchannel gas flow. *J. Micromech. Microengng* **17**, 1695–1702.

SUN, H. & FAGHRI, M. 2003 Effect of surface roughness on nitrogen flow in a microchannel using the direct simulation Monte Carlo method. *Numer. Heat Transfer A-Appl.* **43**, 1–8.

SUN, J. & LI, Z.-X. 2010 Two-dimensional molecular dynamic simulations on accommodation coefficients in nanochannels with various wall configurations. *Comput. Fluids* **39**, 1345–1352.

SUTHERLAND, W. 1895 The viscosity of mixed gases. *Phil. Mag.* **40**, 421–431.

https://doi.org/10.1017/jfm.2012.98 Published online by Cambridge University Press

TANG, G. H., LI, Z., HE, Y. L. & TAO, W. Q. 2007 Experimental study of compressibility, roughness and rarefaction influences on microchannel flow. *Intl J. Heat Mass Transfer* **50**, 2282–2295.

TURNER, S. E., LAM, L. C., FAGHRI, M. & GREGORY, O. J. 2004 Experimental investigation of gas flow in microchannels. *J. Heat Transfer* **126**, 753–763.

YAMAGUCHI, H., HANAWA, T., YAMAMOTO, O., MATSUDA, Y., EGAMI, Y. & NIIMI, T. 2011 Experimental measurement on tangential momentum accommodation coefficient in a single microtube. *Microfluid Nanofluid* **11**, 57–64.

ZOHAR, Y., LEE, S. Y. K., LEE, W. Y., JIANG, L. & TONG, P. 2002 Subsonic gas flow in a straight uniform microchannel. *J. Fluid Mech.* **472**, 125–151.

https://doi.org/10.1017/jfm.2012.98 Published online by Cambridge University Press